Peptide/Nanoparticle Biointerfaces for Multistep Tandem Catalysis

Yuliana Perdomo, * Joseph M. Slocik, * David M. Phillips, * and Marc R. Knecht*, *

[†]Department of Chemistry, University of Miami, Coral Gables, Florida 33146, United States; Dr. J.T. Macdonald Foundation Biomedical Nanotechnology Institute, University of Miami, Miami, Florida 33136, United States

*Materials and Manufacturing Directorate, Air Force Research Laboratory, Dayton, Ohio 45433, United States

ABSTRACT: The realization of multifunctional nanoparticle systems is essential to achieve highly efficient catalytic materials for specific applications; however, their production remains quite challenging. They are typically achieved through the incorporation of multiple inorganic components; however, incorporation of functionality could also be achieved at the organic ligand layer. In this work, we demonstrate the generation of multifunctional nanoparticle catalysts using peptide-based ligands for tandem catalytic functionality. To this end, chimeric peptides were designed that incorporated a Au binding sequence and a catalytic sequence which can drive ester hydrolysis. Using this chimera, Au nanoparticles were prepared, which sufficiently presented the catalytic domain of the peptide to drive tandem catalytic processes occurring at the peptide ligand layer and the Au nanoparticle surface. This work represents unique pathways to achieve multifunctionality from nanoparticle systems tuned by both the inorganic and bio/organic components, which could be highly important for applications beyond catalysis, including theranostics, sensing, and energy technologies.

INTRODUCTION

The design and deployment of multifunctional nanoparticle systems is critical to the advance of multiple applications ranging from theranostics to energy technologies. 1-4 The challenge with this ability, however, lies in the production of the nanoparticles themselves, which requires advanced synthetic strategies to make complex, multicomponent materials. One avenue to achieve multifunctional nanoparticles that is underexplored for energy-based applications focuses on the integration of functional ligands at inorganic particle surfaces.⁵⁻⁷ In this situation, the ligands could be designed to both stabilize the nanoparticle while engendering specific functionalities into the material.8 This could be transformational for nanocatalysts where the catalytic inorganic core component could be coupled with additional functionalities at the ligand surface for secondary catalytic domains, substrate selectivity, etc. Unfortunately, the design of complex ligands for such abilities remains difficult.

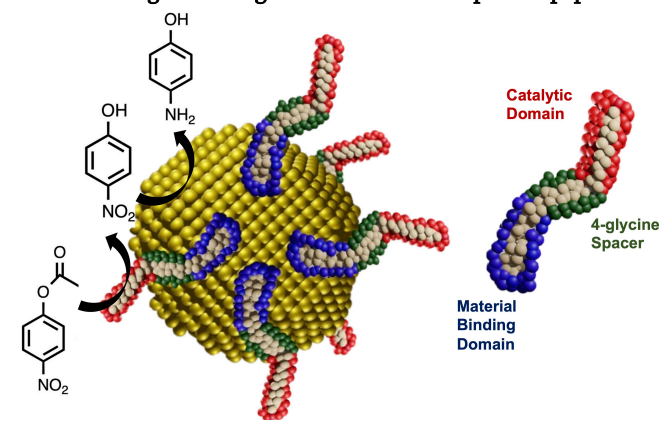
Strategies to prepare functional ligands that bind inorganic nanoparticles are possible; 9-11 however, by necessity, these molecules can be complex. There must be a separate metal surface binding domain and a functionality domain. In this case, the functional domain typically must be presented away from the surface; however, should unanticipated binding of this domain to the surface occur, this could lead to inhibition of the ligand functionality. As such, this makes the design of traditional organic ligands to achieve such capabilities complex and potentially difficult.

As an alternative, bio-inspired approaches could be used to design multifunctional ligands that precisely bind the nanoparticle surface while presenting secondary ligand functionalities. ¹²⁻¹⁷ To this end, peptides have been identified with the ability to bind and stabilize inorganic nanoparticles, including noble metal particles ¹⁸ (e.g., AuBP1, WAGAKRLVLRRE, which binds to Au¹⁹), while additional sequences are known to possess inherent catalytic capabilities. For instance, Ulijn and coworkers have identified the CPN3 peptide (DLRSCTACAVNA),

which can catalyze ester hydrolysis.²⁰ By coupling these peptides together, a new chimeric species could be realized with both a domain responsible for binding the nanoparticle and one for secondary functionality (*e.g.*, catalysis). By anchoring the peptide to a catalytic nanoparticle, multistep, tandem catalysis could be possible, mimicking enzymatic cascades.

In this contribution, we demonstrate a new concept for the design of multifunctional nanoparticle ligands using biomimetic approaches for the generation of single nanoparticle cascade catalysts (Scheme 1). In this regard, a biomolecule was designed that incorporated a Au nanoparticle binding domain (AuBP1) and a catalytic domain (CPN3) into a single chimeric sequence. For this, two specific constructs were made: either the AuBP1-CPN3 or CPN3-AuBP1, which positioned the Au binding domain at either the N- or C-terminus, respectively. These peptides were subsequently employed to generate peptide-capped Au nanoparticles where the biomolecules bound the Au surface through the AuBP1 domain, thus presenting the

Scheme 1. Biointerfaces for tandem catalysis. Catalytic peptides are bound to Au nanoparticles to drive the multistep reaction indicated. At right is a diagram of the multicomponent peptide.



catalytic CPN3 to solution. From this unique structure, multistep cascade-like catalytic functionality was achieved, which is sensitive to the orientation of the two domains in the chimeric bioligand. For the model tandem reaction (Scheme 1), hydrolysis of 4-nitrophenyl acetate (4-NPA) was catalyzed at the peptide interface to generate 4-nitrophenol (4-NP). This intermediate was subsequently converted to 4-aminophenol (4-AP) at the Au surface, demonstrating the multistep functionality. This represents new capabilities from the surface bound ligands, which could be programmed based upon the functionality of the inorganic core. While synergistic activities are demonstrated for catalysis, similar capabilities could be achieved for other applications ranging from drug targeting/delivery to energy harvesting/storage.

EXPERIMENTAL SECTION

Materials

All peptides were commercially synthesized and acquired from Genscript (≥95% purity). Methanol (ACS grade), H₂O₂ (35%), KCl, HCl (ACS grade), and NaOH were purchased from VWR. HAuCl₄ and 4-nitrophenyl acetate (98+%) were both obtained from Alfa Aesar, while 4-nitrophenol (99%) and Na₂HPO₄ were procured from Acros. NaBH₄ (97%) was sourced from Beantown Chemicals and ammonia (25% in water) was obtained from Ward's Scientific. NaH₂PO₄ was purchased from Mallinckrodt Chemicals. For the QCM analysis, all Au sensors were purchased from Biolin and Hellmanex III was obtained from HellmaAnalytics. Finally, Ultrapure Milli-Q water (18.2 MΩ·cm) was used from a Millipore Direct-Q system. All chemicals were used as received.

Quartz Crystal Microbalance (QCM) Binding Analysis. Prior to binding measurements, the Au-coated OCM sensors were exposed to UV/ozone treatment for 10 min and then submerged in a 5:1:1 solution of water, ammonia (25%), and hydrogen peroxide (30%). This mixture was heated at 75 °C for 5 min.²¹ The sensors were then immediately rinsed with water, dried with N₂, and then exposed to UV/ozone treatment for 10 min. Once the sensors were cleaned, they were inserted into a QSense 4 QCM system (Biolin) where water was flowed over the sensor surface for 10 min. Following this time, aqueous solutions of selected peptide concentrations were flowed over the sensors for 30 min to quantify peptide binding to Au. After the binding analysis, Hellmanex III was flowed through the system for 5 min, followed by flowing water for 25 min and then air for 5 min before proceeding to remove sensors. The binding analysis was conducted at five different peptide concentrations ranging from $(0.13 - 1.8) \times 10^{-2}$ mM where previously described methods were used to quantify and calculate the binding free energy of the peptide to Au. 17, 22-23

Nanoparticle Synthesis. Standard methods were employed to prepare the peptide-capped Au nanoparticles. For this, 4.96 mL of 0.1 mM aqueous peptide was combined with 10 μ L of 100 mM aqueous HAuCl₄ followed by stirring at 300 rpm for 15 min. Next, 30 μ L of freshly prepared, aqueous 0.1 M NaBH₄ was added dropwise to the solution. The vial was gently swirled until a color change occurred and then allowed to sit at room temperature for 1 h.

Nanoparticle Characterization. UV-vis analysis was conducted using an Agilent 8453 spectrometer with a 1 cm path

length quartz cuvette. TEM samples were prepared by drop casting 15 μL of a freshly prepared nanoparticle solution onto a lacey carbon-coated 200 Cu-mesh TEM grids (EM Science). The samples were allowed to dry overnight in a desiccator at room temperature. TEM was subsequently conducted using a Talos-200FX microscope operating at 200 kV. Sizing of at least 70 particles per sample was completed to ascertain the average diameter.

4-NPA hydrolysis reactivity. A 119 mM phosphate buffer was prepared at pH 8.0. For the hydrolysis reaction, 1.8 mL of 0.05 mM peptide in buffer was combined with 120 μ L of methanol and 80 μ L of 0.320 mM 4-NPA in methanol. Immediately after substrate addition, the system was monitored at 405 nm via UV-vis analysis for 10 min to quantify 4-NP production over time.

4-NP reduction reactivity. For the reduction of 4-NP, standard reaction procedures were employed. ²⁵⁻²⁸ Briefly, 1.8 mL of 0.05 mM peptide-capped Au nanoparticles in buffer was mixed with 80 μ L of 0.320 mM 4-NP, which stirred for 5 min. To this mixture, 120 μ L of 2.0 M aqueous NaBH₄ was added. The reaction was again quantified via kinetic UV-vis analysis at 405 nm for the consumption of the 4-NP substrate.

RESULTS AND DISCUSSION

For the generation of multistep catalytic nanoparticle system, two different peptide ligands were designed: AuBP1-CPN3 and CPN3-AuBP1 (Table 1). In the first case, the Au binding AuBP1 domain is positioned at the N-terminus, followed by the catalytic CPN3 domain at the C-terminus. For the latter sequence, the order of the two domains were reversed. In both cases, a four glycine spacer was incorporated between the two specific domains. These two sequences were important to identify sequence structural effects that could alter the activity of either domain, which must work independently. In this arrangement, the AuBP1 domain is anticipated to anchor the biomolecule to the Au nanoparticle surface while presenting the secondary catalytic domain to solution. Prior studies have demonstrated that the order of domain incorporation into the chimeric sequence can alter the binding event, necessitating the two sequences.13

Table 1. Peptide sequences, binding free energy values to Au, and nanoparticle diameters.

Name	Sequence	ΔG (kJ/mol)	Diameter (nm)
CPN3	DLRSCTACAVNA	-28.7 ± 0.9	4.1 ± 0.8
*AuBP1	WAGAKRLVLRRE	-40.7 ± 2.1	3.1 ± 0.7
AuBP1-CPN3	WAGAKRLVLRREGGGG- DLRSCTACAVNA	-28.6 ± 1.0	2.7 ± 0.7
CPN3-AuBP1	DLRSCTACAVNAGGGG- WAGAKRLVLRRE	-27.4 ± 1.6	2.8 ± 0.8

^{*}Data for AuBP1 taken from ref 17.

With production of the two chimeric peptides, their affinity, as well as that for the catalytic CPN3 peptide, for Au was measured via QCM (Table 1). From this method, a binding free energy (ΔG) of -28.7 \pm 0.9 kJ/mol was determined for CPN3 binding to the Au surface. Such a value is notably lower than previously observed for the AuBP1 sequence for Au (-40.7 \pm 2.1

kJ/mol).¹⁷ This significant difference in affinity is highly important to ensure that the AuBP1 domain preferentially binds to Au instead of the CPN3 domain.

Quantification of the binding affinity was subsequently performed for the two chimeric peptides, giving rise to ΔG values of -28.6 \pm 1.0 and -27.4 \pm 1.6 kJ/mol for the AuBP1-CPN3 and CPN3-AuBP1, respectively. Such values were lower than that for the AuBP1 peptide binding alone, but were sufficiently strong to ensure binding to the Au nanoparticle surface. Furthermore, with the binding free energy values being similar, this suggests that the order of domain incorporation does not significantly affect the overall affinity; however, it may alter the presentation of the catalytic domain, inhibiting ligand hydrolysis functionality.

With confirmation of peptide affinity for Au, the production of peptide-capped Au nanoparticles was examined. For this, the selected peptide was commixed with two equivalents of HAuCl₄ in water and subsequently reduced with NaBH₄ to generate the final material. Figure 1a presents the UV-vis analysis of the different nanoparticles after reduction. In general, all of the materials demonstrated an increase in absorbance towards lower wavelengths, as anticipated for nanoparticles. Interestingly, only the AuBP1-capped materials displayed a broad plasmon band at 530 nm, consistent with prior results.¹⁷ The other materials did not display a plasmon due to a sufficiently small particle size or lower particle concentration. TEM analysis of the peptide-capped Au nanoparticles was completed to image the final materials. In general, spherical nanoparticles were prepared using the AuBP1-CPN3 (Figure 1b), CPN3-AuBP1, and CPN3 peptides (Supporting Information, Figure S1) with average sizes of 2.7 ± 0.7 , 2.8 ± 0.8 , and 4.1 ± 0.8 nm, respectively. Such sizes were comparable to those prepared using the AuBP1 sequence $(3.1 \pm 0.7 \text{ nm}).^{17}$

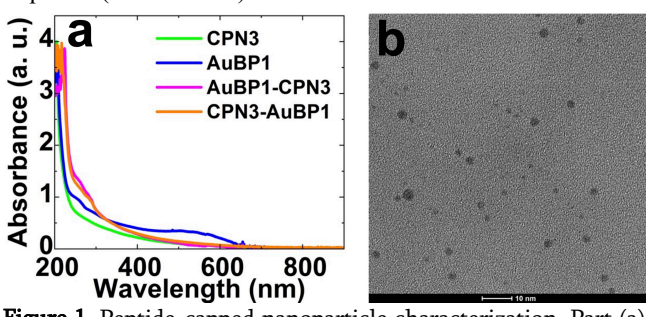


Figure 1. Peptide-capped nanoparticle characterization. Part (a) presents the UV-vis analysis of the materials capped by the indicated peptide, while part (b) presents a TEM image of the AuBP1-CPN3-capped Au nanoparticles.

With confirmation of nanoparticle formation for the chimeric peptides, studies of the catalytic reactivity of the materials were completed. Initially, the first reaction of the tandem process, hydrolysis of 4-NPA to 4-NP (Figure 2a), was studied using the peptides alone. Such studies were important to confirm the inherent reactivity of the CPN3 and chimeric sequences. For this, the reaction was analyzed in phosphate buffer at pH 8, which was observed to be optimal for this reaction. To drive the catalytic process, the 4-NPA substrate was added to the peptide mixture, resulting in rapid hydrolysis to generate the colored 4-NP species. UV-vis spectroscopy was used to observe the growth of the 405 nm 4-NP absorbance to quantify the reaction kinetics. Figure 2b presents the growth in this absorbance as a

function of time for all of the peptide-driven reactions. A degree of background reactivity was noted for the system, giving rise to the observed absorbance at reaction initiation. As a control, the reaction was studied in buffer in the absence of peptide where background hydrolysis was observed with a rate constant (k) of $(2.1 \pm 0.1) \times 10^{-3} \ s^{-1}$ (Figure 2c). This control was conducted under identical conditions (1.8 mL phosphate buffer, pH 8.0, and 200 μ L MeOH), thus the only difference was the lack of peptides to drive the reaction. Note that the rate constants are reported as average values \pm one standard deviation from the mean for triplicate analyses.

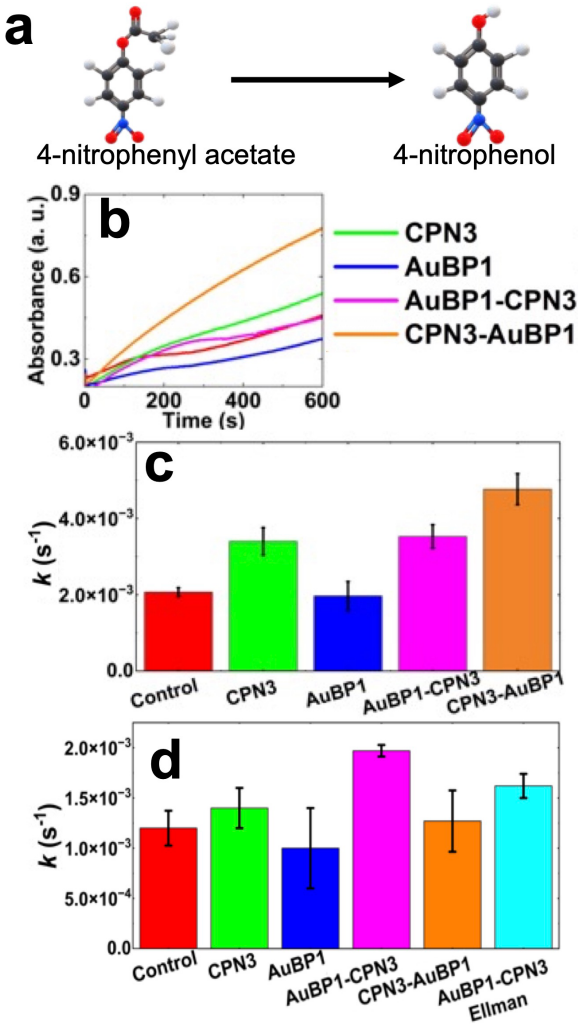


Figure 2. Catalytic analysis of the CPN3-peptide for hydrolysis of 4-NPA. Part (a) presents the reaction, while part (b) displays the UV-vis analysis at 405 nm of the reaction driven by the indicated peptide. Part (c) presents the k values for the peptide driven reaction, while part (d) shows the rate constants for the reaction driven by the peptide adsorbed onto the Au nanoparticle surface.

When the CPN3-based peptide reactivity was analyzed, enhanced reaction rate constants were observed compared to the background (Figure 2c). For the CPN3 parent peptide reactivity, a k value of $(3.4 \pm 0.4) \times 10^{-3} \text{ s}^{-1}$ was quantified, which was slightly higher than prior results²⁰ due to differences in reaction conditions. This represents a 62% enhancement as compared to the background. Ulijn and coworkers suggested that the basis

for this reactivity likely arises from the serine and cysteine residues in the sequence;²⁰ however, further studies are required to confirm this theory. For an additional control analysis, the reactivity of the AuBP1 peptide was also studied, which demonstrated activity consistent with the background ($k = (2.0 \pm 0.4)$ \times 10⁻³ s⁻¹). As anticipated, no reactivity associated with the Au binding domain was observed. When the hydrolysis reactivity of the chimeras was analyzed, rate constant values of (3.5 ± 0.3) \times 10⁻³ and (4.8 ± 0.4) \times 10⁻³ s⁻¹ were noted for the AuBP1-CPN3 and CPN3-AuBP1 peptides, respectively. Such values suggest that incorporation of the catalytic domain into the larger biomolecule did not inhibit reactivity and may actually increase the catalytic capability for the CPN3-AuBP1. Prior studies of different materials binding peptides have demonstrated changes in binding affinity and adsorbed structure when conjugated to secondary functionalities. ^{13,14,29} These differences arise from changes to the overall structure of the biomolecule, which could be occurring in the CPN3-AuBP1 chimera to promote increased reactivity; however, additional analyses are required to confirm such an effect.

The hydrolysis reactivity of the peptides once immobilized on the Au nanoparticle surface was subsequently studied (Figure 2d). For this, identical reaction procedures were employed; however, using the nanoparticles, the pH of the reaction system decreased to 7.7. At this lower pH, slightly diminished background reactivity was noted from the control in the absence of the nanoparticles, with a k value of $(1.2 \pm 0.2) \times 10^{-3} \, \text{s}^{-1}$. For the Au nanoparticles capped with either the CPN3 or AuBP1 peptides, similar degrees of reactivity as compared to the control were noted with rate constants of $(1.4 \pm 0.2) \times 10^{-3}$ and $(1.0 \pm 0.4) \times 10^{-3} \, \text{s}^{-1}$, respectively. This was anticipated for the non-reactive AuBP1 and for the CPN3, as well. For CPN3, the reactivity was suppressed due to the binding event between the peptide and the Au nanoparticle, preventing exposure of the biomolecule to solution for reactivity.

Reactivity analysis for the hydrolysis of 4-NPA using the nanoparticles capped with the two chimeric peptides provided highly interesting results. For the AuBP1-CPN3-capped Au nanoparticles, a k value of $(2.0 \pm 0.06) \times 10^{-3}$ s⁻¹ was noted, which is higher than the background (67% enhancement). This suggests that the peptide-based reactivity was retained in this system where the CPN3 catalytic domain was sufficiently presented to solution to drive 4-NPA hydrolysis. Interestingly, when the second chimeric peptide-capped Au nanoparticle (CPN3-AuBP1) was studied for the reaction, a rate constant equivalent to the background reaction was observed ($k = (1.3 \pm$ 0.3) × 10^{-3} s⁻¹). This indicates that for this chimeric peptide, the catalytic domain was in sufficient contact with the Au surface, thus preventing reactivity. As such, the order of domain incorporation into the chimeric biomolecule has a significant effect on the peptide surface adsorbed structure to inhibit ligand hydrolysis reactivity.

It is quite interesting that such different reactivity for 4-NPA hydrolysis was observed from the two chimera once adsorbed to the Au nanoparticle surface. This indicates that exposure of the catalytic domain was achieved for the AuBP1-CPN3 system; however, for the CPN3-AuBP1 sequence, the catalytic domain was presented in a way that prohibits reactivity. Prior studies have demonstrated that changes to the overall peptide sequence can have significant effects on the structure of the biomolecule in the surface adsorbed state. ^{13, 14, 29} This structural change as a function of domain order in the chimera could have

dramatic implications on the reactivity, giving rise to the different hydrolysis capabilities for the two chimera-capped Au nanoparticles (*i.e.*, reactivity for AuBP1-CPN3 and no reactivity for CPN3-AuBP1). Ulijn and coworkers have indicated that the cysteine and serine residues of CPN3 are potentially the basis for the reactivity,²⁰ thus they are more likely to be exposed for the reactive AuBP1-CPN3 system as compared to the catalytically inactivity CPN3-AuBP1.

To confirm this effect of the cysteine residues, derivatization of the thiols in the free CPN3 peptide was completed using the Ellman's reagent. ³⁰ Employing the derivatized free peptide, no hydrolysis reactivity above the background was noted, confirming the role of the cysteine residue. Next, the AuBP1-CPN3-capped Au nanoparticles were derivatized using the Ellman's reagent. Should the cysteines not be adsorbed to the Au nanoparticle, they would be susceptible to derivatization, thus leading to diminished hydrolysis reactivity. Using these derivatized Au nanoparticles, a k value of $(1.6 \pm 0.1) \times 10^{-3} \, \text{s}^{-1}$ was observed (Figure 2d – light blue bar), which was notably lower than for the underivatized materials. This result demonstrates that the cysteine residues were exposed at the hydrolysis active site, which upon derivatization, leads to their catalytic deactivation.

After elucidating the reactivity of the peptide ligands for the first step in the tandem reaction, the catalytic activity of the underlying Au core for the second step in the process (4-NP

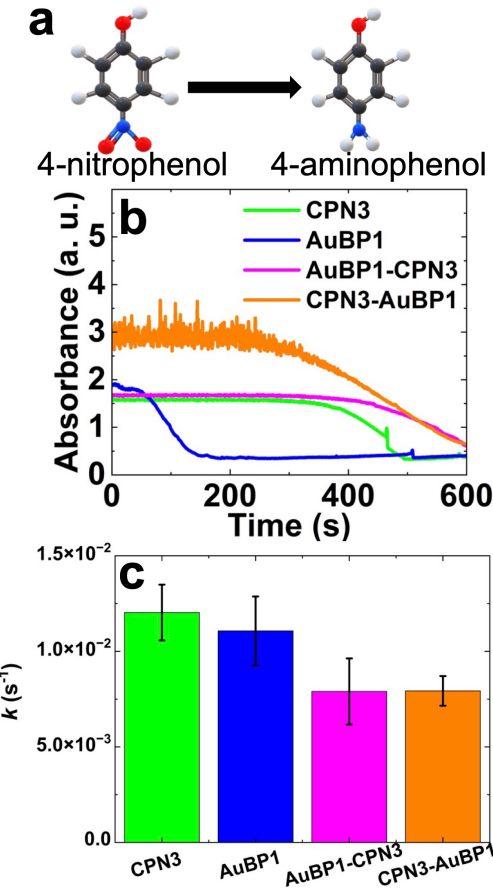


Figure 3. Catalytic analysis of the peptide-capped Au nanoparticles for the reduction of 4-NP to 4-AP. Part (a) displays the anticipated reaction, while part (b) presents the change in absorbance at 405 nm throughout the reaction. Part (c) shows the calculated *k* values for the reaction after the lag time using the Au nanoparticles capped with the indicated peptides.

reduction to 4-AP – Figure 3a) was examined. This reaction is well-known to occur directly on the metallic surface. ²⁵ To monitor the reaction, consumption of the 4-NP intermediate was monitored via a decrease in the 405 nm absorbance as a function of time. Figure 3b plots this analysis. For each reaction system, a lag time was noted that was likely due to O_2 consumption in the solution; ²⁶ however, quantification of k values was determined immediately after completion of the lag time. For all of the systems in the absence of nanoparticles, no reaction was observed, as anticipated. When the peptide-capped Au nanoparticles were studied, rapid 4-NP reduction was noted. For the two nanoparticle control systems capped with the CPN3 and AuBP1 peptides, reaction k values of $(1.2 \pm 0.2) \times 10^{-2}$ and $(1.1 \pm 0.2) \times 10^{-2}$ were quantified, respectively (Figure 3c).

Interestingly, when the nanoparticles capped with the two chimeric peptides were employed to drive the reduction reaction, diminished reactivity was noted, giving rise to a rate constant of $(7.9 \pm 1.7) \times 10^{-3} \text{ s}^{-1}$ for the AuBP1-CPN3-capped particles and $(7.9 \pm 0.08) \times 10^{-3} \text{ s}^{-1}$ for the CPN3-AuBP1-capped materials. The diminished reactivity for the second step of the tandem process was somewhat surprising; it may be related to the increased amount of biological ligand present on the nanoparticle that could inhibit access of the 4-NP substrate to the catalytic metal surface. Nevertheless, 4-NP reduction reactivity was observed from these species, confirming that they could be used for the second step of the tandem process.

With confirmation of reactivity for both 4-NPA hydrolysis and 4-NP reduction, the tandem reactivity for the AuBP1-CPN3-capped Au nanoparticles was examined (Figure 4). Since the CPN3-AuBP1-based system demonstrated negligible reactivity for 4-NPA hydrolysis, its reactivity for the tandem reaction was not further explored. Using the AuBP1-CPN3-capped

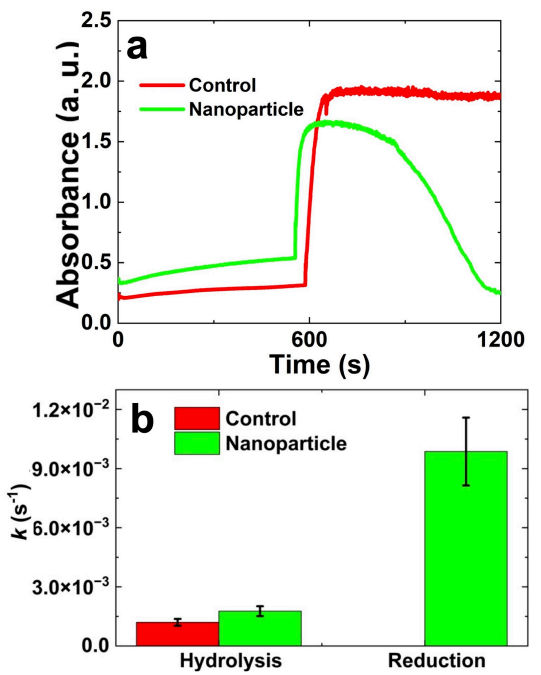


Figure 4. Tandem catalytic analysis of the AuBP1-CPN3-capped Au nanoparticles. Part (a) presents the absorbance at 405 nm throughout the reaction where 4-NPA hydrolysis is occurring prior to 600 s, which is followed by 4-NP reduction after this time point. Part (b) presents the rate constant value calculated for the nanoparticles and control for both steps of the process.

materials, the tandem process was initiated by driving 4-NPA hydrolysis. Once the process reached near completion at ${\sim}600$ s, NaBH₄ was injected into the system to initiate reduction of the 4-NP intermediate to generate the 4-AP final product. Note that the steps must be separated to facilitate UV-vis monitoring of the reaction phases.

Figure 4a presents the change in absorbance intensity as a function of time at 405 nm. This absorbance should increase as a function of 4-NP intermediate production during the first step of the tandem process, which it does for both the control and AuBP1-CPN3-capped Au nanoparticles. As anticipated (Figure 4b), the k values for the first step were greater for the nanoparticle catalyzed system ((1.8 \pm 0.3) \times 10⁻³ s⁻¹) versus the control ((1.2 \pm 0.2) \times 10⁻³ s⁻¹).

After \sim 600 s, injection of NaBH₄ occurred, giving rise to a significant increase in absorbance. Such a jump arises from deprotonation of the 4-NP intermediate to generate 4-nitrophenolate, which has a significantly higher molar absorptivity constant at 405 nm.³¹ To confirm this effect, the pH of the reaction system after NaBH₄ addition was measured to be \sim 10, which would be sufficient to fully deprotonate 4-NP. After a lag time of \sim 400 s for the tandem catalyst system, rapid 4-NP reduction was observed to generate the 4-AP final product. For this process, significant catalytic turnover was observed (Figure 4a), giving rise to a k value of $(9.9 \pm 1.7) \times 10^{-3}$ s⁻¹. For the control reaction in the absence of the nanoparticles, no change in absorbance of the 4-NP intermediate was noted over the time frame of the study, consistent with the lack of reactivity.

To further examine the tandem functionality of the AuBP1-CPN3-based system, a new reaction was examined wherein free CPN3 peptide was mixed in solution with AuBP1-capped Au nanoparticles. Using this system, the two catalytic regions were physically separated. Identical procedures were subsequently employed as in Figure 4 where the free CPN3 peptides drove 4-NPA hydrolysis to produce 4-NP. After ~600 s, NaBH₄ was added to drive the second step of the reaction (4-NP reduction to 4-AP). In this system, the rate constant for 4-NPA hydrolysis was $(1.8 \pm 0.4) \times 10^{-3}$ s⁻¹ and for 4-NP reduction was (1.2 ± 0.2) \times 10⁻² s⁻¹. Such values were consistent with the k values observed for the tandem catalysts. Taken together, this confirms two key factors about the chimeric-based system: Incorporation of the CPN3 into the CPN3-AuBP1 peptide, and passivation of the chimera onto the Au nanoparticle, does not diminish or inhibit hydrolysis activity. Unfortunately, simultaneous initiation of both steps of the reaction could not be completed due to the UV-vis reaction quantification method that relied upon the 405 nm absorbance for intermediate production and consumption.

In addition, the effect of the 4-NPA concentration on the tandem reactivity of the AuBP1-CPN3-capped Au nanoparticles was also analyzed to determined changes in reaction kinetics. In this case, five substrate concentrations were explored: 0.1, 0.2, 0.32, 0.5, and 0.6 mM. Note that 0.32 mM is the standard reaction concentration used above. As shown in Figure 5a, at a 4-NPA concentration of 0.1 mM, the k value for the peptidecatalyzed hydrolysis reaction was $(0.8 \pm 0.1) \times 10^{-3} \, \mathrm{s}^{-1}$. As the 4-NPA concentration increased, larger rate constants were observed, giving rise to a maximum value of $(2.5 \pm 0.1) \times 10^{-3} \, \mathrm{s}^{-1}$ at 0.6 mM substrate. In all case, the k values were greater for the peptide-catalyzed hydrolysis reaction as compared to the peptide-free control reactions, confirming that the biomolecules were increasing the reaction rates. From this analysis, it was

evident that a logarithmic increase in rate constants was observed as a function of substrate concentration. This suggests that some type of binding of the 4-NPA substrate to the peptidecapped Au nanoparticles is required to drive the reaction, similar to an enzyme. Such results are different from the prior observations of Ulijn and colleagues, which suggested that binding was not required for the free peptide in solution.²⁰ Additional analysis of the catalytic parameters of the peptide-capped system are presently being explored separately.

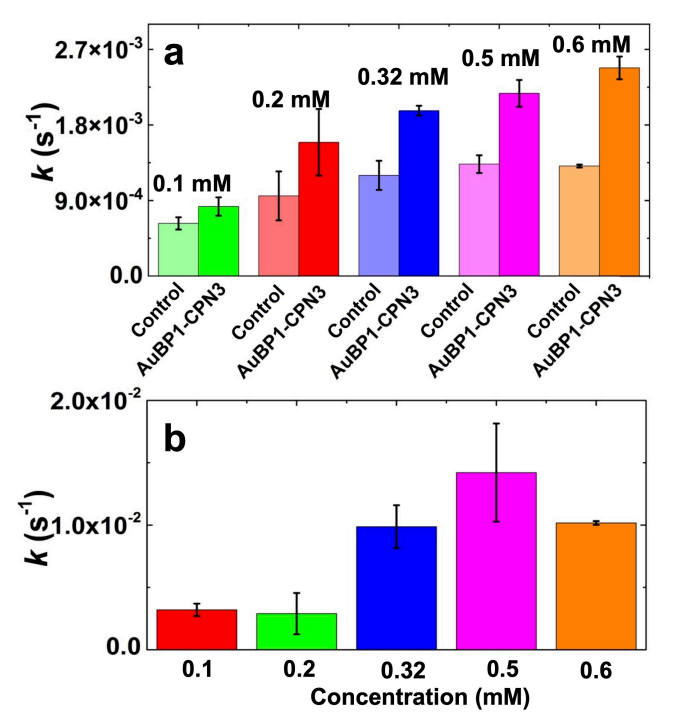


Figure 5. Effects of substrate concentration on catalytic reactions. Part (a) presents the analysis for changes in 4-NPA concentration for ester hydrolysis, while part (b) displays the results for reduction of 4-NP produced in part (a).

After completion of the 4-NPA hydrolysis, injection of the NaBH₄ was used to drive the second step of the reaction at the different substrate concentration. Figure 5b presents the k values for this step obtained during the production of 4-AP from 4-NP. In this case, a relatively low rate constant of $(3.2 \pm 0.5) \times 10^{-3} \, \text{s}^{-1}$ was obtained at a starting concentration of 0.1 mM; however, at the two higher concentrations, equivalent k values were obtained of $\sim 9 \times 10^{-3} \, \text{s}^{-1}$. Taken together, this suggests that the process was sensitive to the starting material concentration, particularly for the hydrolysis step.

To achieve tandem catalytic functionality, the present materials exploit both the catalytic inorganic nanomaterial as well as catalytic ligands displayed at the surface. Such capabilities are different from other nanocatalysts where multiple inorganic components are exploited for tandem catalytic activity. ^{2, 32-33} One comparable system was previously described by Filice *et. al* that exploited a lipase enzyme (CAL-B) to generate Pd nanoparticles for tandem functionality. ³⁴ In this case, the lipase adsorbed to a Pd nanoparticle drove hydrolysis of 4-nitrobutyrate, where the nitro group was subsequently reduced at the Pd surface. In this case, the enzyme also served to reduce Pd²⁺ ions to generate the nanoparticles. While tandem reactivity was observed, nanoparticle production/stabilization led to diminished

enzymatic activity. In addition, the system is likely to be sensitive to the reaction conditions due to the requisite secondary structure of the enzyme. In separate work, Mikolajczak and Koksh were able to achieve similar tandem catalytic reactivity using a catalytic peptide anchored on a Au nanoparticle surface. 35 The key differences here is that the peptides were anchored to the Au particle via thiol residues, which could poison the metal surface to inhibit reactivity. Such binding is also not specific (as achieved using the AuBP1 binding domains presented herein), which could be present issues in displaying the catalytic domain. Interestingly, for this peptide, it was not catalytically reactive until bound to the particle surface; when free in solution, it was inactive. This suggests that the peptide required more complex interactions to achieve catalytic turnover as compared to the present system that simplifies the tandem catalytic activity.

Using the AuBP-CPN3-based materials, significant reactivity associated with the surface bound peptide was maintained when adsorbed to the Au nanoparticle. In addition, no secondary structure or cooperative interpeptide interactions were required for the peptide to drive the reaction, suggesting that the peptide-based system is amenable to changes in the reaction conditions. For the other two comparable systems, secondary structure (enzyme) and interpeptide interactions (peptides) are required, which are likely to be highly sensitive to the ligand interfacial morphology and solution conditions, both of which could be overcome in the present system. Finally, based upon the chimera structure, highly controlled docking of the peptide to the particle surface can be achieved to ensure efficient presentation of the secondary functionality to optimize the properties.

CONCLUSION

In conclusion, this work has demonstrated a unique tandem catalytic functionality, integrating reactivity from both the catalytic nanoparticles and catalytic peptides. The specific reactivities were tuned to work synergistically to achieve tandem functionality. The ability to generate the functional ligands revolved around biological recognition capabilities, ensuring specific ligand binding to the Au nanoparticles (AuBP1) and presentation of the catalytic CPN3 domain. This specificity is key to achieving functional ligands on nanoparticle surfaces to achieve multifunctional capabilities. The activities of peptides are expansive and can be tuned to act synergistically with the properties of the underlying nanoparticle composition, thus allowing for the development of multifunctional bio-based nanoparticle system for activities beyond catalysis.

AUTHOR INFORMATION

Corresponding Author

*MRK - knecht@miami.edu

Author Contributions

The manuscript was written through contributions of all authors.

Supporting Information

Additional TEM images and sizing analyses, and UV-vis kinetic analysis for nanoparticle-driven 4-NPA hydrolysis. The Supporting Information is available free of charge at XXX.

Funding Sources

This material is based upon work supported by the National Science Foundation under Grant No. 2203862 (MRK).

REFERENCES

- 1. Wang, D.; Liu, B.; Ma, Y.; Wu, C.; Mou, Q.; Deng, H.; Wang, R.; Yan, D.; Zhang, C.; Zhu, X., A Molecular Recognition Approach To Synthesize Nucleoside Analogue Based Multifunctional Nanoparticles for Targeted Cancer Therapy. *J. Am. Chem. Soc.* **2017**, *139*, 14021-14024.
- 2. Su, J.; Xie, C.; Chen, C.; Yu, Y.; Kennedy, G.; Somorjai, G. A.; Yang, P., Insights into the Mechanism of Tandem Alkene Hydroformylation over a Nanostructured Catalyst with Multiple Interfaces. *J. Am. Chem. Soc.* **2016**, *138*, 11568-11574.
- 3. Yamada, Y.; Tsung, C.-K.; Huang, W.; Huo, Z.; Habas, S. E.; Soejima, T.; Aliaga, C. E.; Somorjai, G. A.; Yang, P., Nanocrystal bilayer for tandem catalysis. *Nat. Chem.* **2011**, *3*, 372-376.
- 4. Cheng, L.; Wang, C.; Feng, L.; Yang, K.; Liu, Z., Functional Nanomaterials for Phototherapies of Cancer. *Chem. Rev.* **2014**, *114*, 10869-10939.
- 5. Mikolajczak, D. J.; Berger, A. A.; Koksch, B., Catalytically Active Peptide–Gold Nanoparticle Conjugates: Prospecting for Artificial Enzymes. *Angew. Chem. Int. Ed.* **2020**, 59, 8776-8785.
- 6. Neri, S.; Garcia Martin, S.; Pezzato, C.; Prins, L. J. Photoswitchable Catalysis by a Nanozyme Mediated by a Light-Sensitive Cofactor. *JACS* **2017**, 139, 1794-1797.
- 7. Chen, J. L. Y.; Pezzato, C.; Scrimin, P.; Prins, L. J. Chiral Nanozymes—Gold Nanoparticle-Based Transphosphorylation Catalysts Capable of Enantiomeric Discrimination. *Chem. Eur. J.* **2016**, 22, 7028-7032.
- 8. Unal Gulsuner, H.; Ceylan, H.; Guler, M. O.; Tekinay, A. B., Multi-Domain Short Peptide Molecules for in Situ Synthesis and Biofunctionalization of Gold Nanoparticles for Integrin-Targeted Cell Uptake. *ACS Appl. Mater. Interfaces* **2015**, *7*, 10677-10683.
- 9. Bonomi, R.; Selvestrel, F.; Lombardo, V.; Sissi, C.; Polizzi, S.; Mancin, F.; Tonellato, U.; Scrimin, P., Phosphate Diester and DNA Hydrolysis by a Multivalent, Nanoparticle-Based Catalyst. *J. Am. Chem. Soc.* **2008**, *130*, 15744-15745.
- 10. Lyu, Y.; Scrimin, P., Mimicking Enzymes: The Quest for Powerful Catalysts from Simple Molecules to Nanozymes. *ACS Catal.* **2021**, *11*, 11501-11509.
- 11. Mout, R.; Ray, M.; Yesilbag Tonga, G.; Lee, Y.-W.; Tay, T.; Sasaki, K.; Rotello, V. M., Direct Cytosolic Delivery of CRISPR/Cas9-Ribonucleoprotein for Efficient Gene Editing. *ACS Nano* **2017**, *11*, 2452-2458.
- 12. Yazici, H.; O'Neill, M. B.; Kacar, T.; Wilson, B. R.; Oren, E. E.; Sarikaya, M.; Tamerler, C., Engineered Chimeric Peptides as Antimicrobial Surface Coating Agents toward Infection-Free Implants. *ACS Appl. Mater. Interfaces* **2016**, *8*, 5070-5081.
- 13. Briggs, B. D.; Palafox-Hernandez, J. P.; Li, Y.; Lim, C.-K.; Woehl, T. J.; Bedford, N. M.; Seifert, S.; Swihart, M. T.;

- Prasad, P. N.; Walsh, T. R.; Knecht, M. R., Toward a modular multi-material nanoparticle synthesis and assembly strategy via bionanocombinatorics: bifunctional peptides for linking Au and Ag nanomaterials. *Phys. Chem. Chem. Phys.* **2016**, *18*, 30845-30856.
- 14. Jin, R.; Brljak, N.; Sangrigoli, R.; Walsh, T. R.; Knecht, M. R., Achieving regioselective materials binding using multidomain peptides. *Nanoscale* **2022**, *14*, 14113-14121.
- 15. Kacar, T.; Ray, J.; Gungormus, M.; Oren, E. E.; Tamerler, C.; Sarikaya, M., Quartz binding peptides as molecular linkers towards fabricating multifunctional micropatterned substrates. *Adv. Mater.* **2009**, *21*, 295-299.
- 16. Kim, Y.; Macfarlane, R. J.; Jones, M. R.; Mirkin, C. A., Transmutable nanoparticles with reconfigurable surface ligands. *Science* **2016**, *351*, 579-582.
- 17. Nguyen, M. A.; Hughes, Z. E.; Liu, Y.; Li, Y.; Swihart, M. T.; Knecht, M. R.; Walsh, T. R., Peptide-Mediated Growth and Dispersion of Au Nanoparticles in Water via Sequence Engineering. *J. Phys. Chem. C***2018**, *122*, 11532-11542.
- 18. Walsh, T. R.; Knecht, M. R., Biointerface Structural Effects on the Properties and Applications of Bioinspired Peptide-Based Nanomaterials. *Chem. Rev.* **2017**, *117*, 12641-12704.
- 19. Hnilova, M.; Oren, E. E.; Seker, U. O.; Wilson, B. R.; Collino, S.; Evans, J. S.; Tamerler, C.; Sarikaya, M., Effect of molecular conformations on the adsorption behavior of gold-binding peptides. *Langmuir* **2008**, *24*, 12440-5.
- 20. Maeda, Y.; Javid, N.; Duncan, K.; Birchall, L.; Gibson, K. F.; Cannon, D.; Kanetsuki, Y.; Knapp, C.; Tuttle, T.; Ulijn, R. V.; Matsui, H., Discovery of Catalytic Phages by Biocatalytic Self-Assembly. *J. Am. Chem. Soc.* **2014**, *136*, 15893-15896.
- 21. Kern, W., Cleaning solution based on hydrogen peroxide for use in silicon semiconductor technology. *RCA rev.* **1970**, *31*, 187-206.
- 22. Tang, Z.; Palafox-Hernandez, J. P.; Law, W. C.; Hughes, Z. E.; Swihart, M. T.; Prasad, P. N.; Knecht, M. R.; Walsh, T. R., Biomolecular recognition principles for bionanocombinatorics: an integrated approach to elucidate enthalpic and entropic factors. *ACS Nano* **2013**, *7*, 9632-46.
- 23. Tamerler, C.; Oren, E. E.; Duman, M.; Venkatasubramanian, E.; Sarikaya, M., Adsorption kinetics of an engineered gold binding Peptide by surface plasmon resonance spectroscopy and a quartz crystal microbalance. *Langmuir* **2006**, *22*, 7712-8.
- 24. Li, Y.; Tang, Z.; Prasad, P. N.; Knecht, M. R.; Swihart, M. T., Peptide-mediated synthesis of gold nanoparticles: effects of peptide sequence and nature of binding on physicochemical properties. *Nanoscale* **2014**, *6*, 3165-3172.
- 25. Wunder, S.; Polzer, F.; Lu, Y.; Mei, Y.; Ballauff, M., Kinetic Analysis of Catalytic Reduction of 4-Nitrophenol by Metallic Nanoparticles Immobilized in Spherical

- Polyelectrolyte Brushes. *J. Phys. Chem. C* **2010**, *114*, 8814-8820.
- 26. Neal, R. D.; Hughes, R. A.; Sapkota, P.; Ptasinska, S.; Neretina, S., Effect of Nanoparticle Ligands on 4-Nitrophenol Reduction: Reaction Rate, Induction Time, and Ligand Desorption. *ACS Catal.* **2020,** *10*, 10040-10050.
- 27. Lawrence, R. L.; Scola, B.; Li, Y.; Lim, C.-K.; Liu, Y.; Prasad, P. N.; Swihart, M. T.; Knecht, M. R., Remote Optically Controlled Modulation of Catalytic Properties of Nanoparticles through Reconfiguration of the Inorganic/Organic Interface. *ACS Nano* **2016**, *10*, 9470-9477.
- 28. Olagunju, M. O.; Liu, Y.; Frenkel, A. I.; Knecht, M. R., Atomically Resolved Characterization of Optically Driven Ligand Reconfiguration on Nanoparticle Catalyst Surfaces. *ACS Appl. Mater. Interfaces* **2021**, *13*, 44302-44311.
- 29. Brljak, N.; Jin, R.; Walsh, T. R.; Knecht, M. R., Selective manipulation of peptide orientation on hexagonal boron nitride nanosheets. *Nanoscale* **2021**, *13*, 5670-5678.
- 30. Moser, M.; Behnke, T.; Hamers-Allin, C.; Klein-Hartwig, K.; Falkenhagen, J.; Resch-Genger, U. Quantification of PEG-Maleimide Ligands and Coupling Efficiencies on Nanoparticles with Ellman's Reagent. *Anal. Chem.* **2015**, *87*, 9376-9383.
- 31. Rufo, C. M.; Moroz, Y. S.; Moroz, O. V.; Stöhr, J.; Smith, T. A.; Hu, X.; DeGrado, W. F.; Korendovych, I. V.,

- Short peptides self-assemble to produce catalytic amyloids. *Nat. Chem.* **2014**, *6*, 303-9.
- 32. Chen, L.; Qi, Z.; Peng, X.; Chen, J.-L.; Pao, C.-W.; Zhang, X.; Dun, C.; Young, M.; Prendergast, D.; Urban, J. J.; Guo, J.; Somorjai, G. A.; Su, J., Insights into the Mechanism of Methanol Steam Reforming Tandem Reaction over CeO2 Supported Single-Site Catalysts. *J. Am. Chem. Soc.* **2021**, *143*, 12074-12081.
- 33. Xie, C.; Niu, Z.; Kim, D.; Li, M.; Yang, P., Surface and Interface Control in Nanoparticle Catalysis. *Chem. Rev.* **2020**, *120*, 1184-1249.
- 34. Filice, M.; Marciello, M.; Morales, M. d. P.; Palomo, J. M., Synthesis of heterogeneous enzyme–metal nanoparticle biohybrids in aqueous media and their applications in C–C bond formation and tandem catalysis. *Chem. Comm.* **2013**, *49*, 6876-6878.
- 35. Mikolajczak, D. J.; Koksch, B., Peptide-Gold Nanoparticle Conjugates as Sequential Cascade Catalysts. *ChemCatChem* **2018**, *10*, 4324-4328.

FOR TABLE OF CONTENTS USE ONLY

